Contents lists available at ScienceDirect

Applied Radiation and Isotopes

journal homepage: www.elsevier.com

Comparison of methods for $H^*(10)$ calculation from measured $LaBr_3(Ce)$ detector spectra

A. Vargas[a, *], N. Cornejo[b], A. Camp[a]

[a] Institut de Tècniques Energètiques (INTE), Universitat Politècnica de Catalunya (UPC), Barcelona, Spain
[b] Centro de Investigaciones Energéticas, Medioambientales y Tecnológicas (CIEMAT), Madrid, Spain

ARTICLE INFO

ABSTRACT

The Universitat Politecnica de Catalunya (UPC) and the Centro de Investigaciones Energéticas, Medioambientales y Tecnológicas (*CIEMAT)* have evaluated methods based on stripping, conversion coefficients and Maximum Likelihood Estimation using Expectation Maximization (ML-EM) in calculating the $H^*(10)$ rates from photon pulse-height spectra acquired with a spectrometric $LaBr_3(Ce)(1.5'' \times 1.5'')$ detector. There is a good agreement between results of the different $H^*(10)$ rate calculation methods using the spectra measured at the UPC secondary standard calibration laboratory in Barcelona. From the outdoor study at ESMERALDA station in Madrid, it can be concluded that the analysed methods provide results quite similar to those obtained with the reference RSS ionization chamber. In addition, the spectrometric detectors can also facilitate radionuclide identification.

1. Introduction

Within the framework of the European project "Metrology for radiological early warning networks in Europe" (MetroERM. http://earlywarning-emrp.eu/), one of the main aims is to obtain the ambient dose equivalent rate ($H^*(10)$ rate) from spectra acquired by spectrometric detectors that could be installed in early warning networks in the near future. In the present work, the spectrometric $LaBr_3(Ce)(1.5'' \times 1.5'')$ SpectroTRACER detector from Saphymo Company was chosen for a comparison of implemented $H^*(10)$ calculation methods within the framework of this European project.

Different methods can be used to calculate $H^*(10)$ rate from the measured pulse-height spectrum. A description of these methods can be found in Dombrowski et al., 2014. In the present paper, different methods included in computer codes that we developed at the INTE and CIEMAT are compared using the spectra acquired by the SpectroTRACER.

The UPC uses two methodologies to calculate $H^*(10)$ rate from acquired photon spectra: the stripping and conversion coefficients methods, both implemented in the '*spc2dose*' computer code. CIEMAT applies the ML-EM method implemented in the '*DET-H10R*' code for deconvolution of the measured pulse-height spectra and the calculation of the corresponding $H^*(10)$ rates. At present, no specific references are available on these codes.

Detector response matrices required in the above-mentioned computer codes can be calculated using any available Monte Carlo (MC) simulation package provided that the response matrix is introduced into the code following a pre-defined format. The response matrices in this study were calculated by using MC simulations with the software packages PENELOPE/penEasy (Sempau et al., 2011) for '*spc2dose*' and MCNPX (Hendricks et al., 2008) for '*DET-H10R*'.

In order to carry out the study, the spectrometric detector was irradiated with different energies and $H^*(10)$ rates at the UPC secondary standard calibration and dosimetry laboratory (LCD) using ^{241}Am, ^{137}Cs and ^{60}Co sources. The $H^*(10)$ rates that were obtained by the above mentioned methods and those provided by the $LaBr_3$ $(1.5'' \times 1.5'')$ detector using the manufacturer's calculation algorithm were compared with the reference values provided by the LCD. The spectrometric detector was then installed at the ESMERALDA reference station, located at the CIEMAT premises in Madrid, and continuous spectra were acquired at regular 10-min time intervals for one year. A long-term comparison of the $H^*(10)$ rates calculated with the three studied methods at the reference station was carried out.

* Corresponding author.
Email address: arturo.vargas@upc.edu (A. Vargas)

https://doi.org/10.1016/j.apradiso.2018.03.026
Received 22 February 2017; Received in revised form 20 March 2018; Accepted 30 March 2018
Available online xxx
0969-8043/

2. Methodology

2.1. $LaBr_3$ (Ce)(1.5″ × 1.5″) detector description

The geometries and materials for the $LaBr_3$ (1.5″ × 1.5″) SpectroTRACER were obtained from the manufacturer. Fig. 1 shows the schematic diagram of the detector using the GVIEW2D tool included in the PENELOPE Monte Carlo code (Salvat, 2015). It should be noted that in the GVIEW2D tool all materials are considered as solids, including air, which is in disagreement with layouts described by technical drawings.

2.2. Irradiations at the LCD facility

The codes that we had developed were applied to experimental spectra acquired by the $LaBr_3$(Ce) detector during the irradiations at LCD. The LCD has been accredited by the Spanish National Accredita-

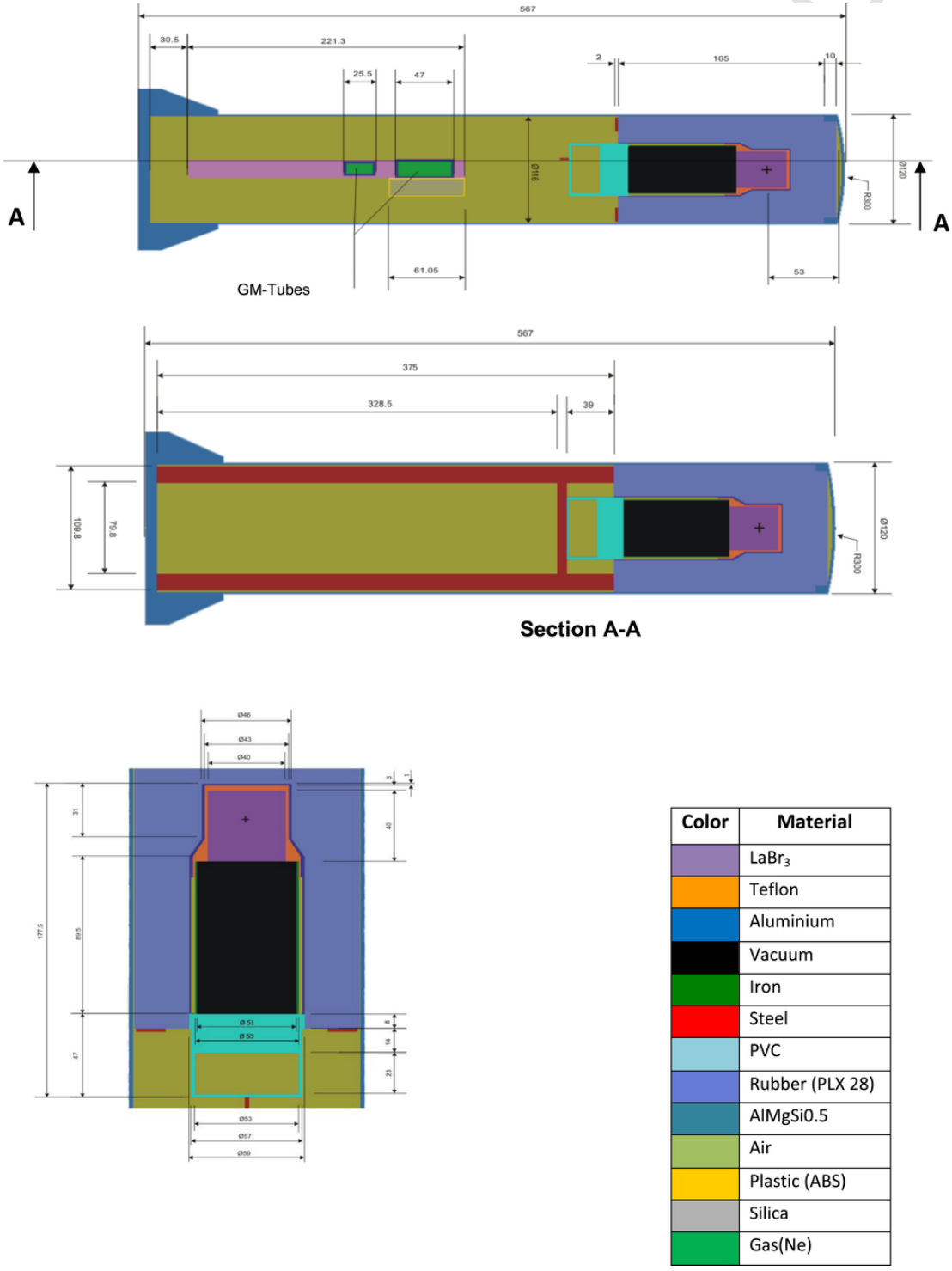

Fig. 1. Geometry and materials of the $LaBr_3$ (1.5″ × 1.5″) SpectroTRACER model from the Saphymo spectrometric monitor.

tion Agency (ENAC) following the ISO 17025 standard (http://inte.upc.edu/en/services/calibration-and-dosimetry).

The detector was irradiated at different energies and ambient dose equivalent rates using ^{241}Am, ^{137}Cs and ^{60}Co sources. The acquisition time was 5 min for each spectrum. Table 1 shows some basic details of the performed irradiations.

2.3. ESMERALDA reference station

The spectrometric detector was installed at the ESMERALDA station and spectra were recorded at 10-min intervals throughout 2016. The ESMERALDA station was set up on CIEMAT premises in 1996 as a reference site for the study of radiation instruments which would subsequently be used to perform continuous or long-term studies of environmental radiation and airborne radioactivity. Different passive and active devices continuously monitor the environmental external radiation dose. In addition, meteorological parameters, radon progeny air concentrations and radioactive aerosols are also monitored by specific instruments. A more detailed description of this station, including the instruments and the measurements carried out can be found elsewhere (Sáez Vergara et al., 1996, 2004).

Table 1
List of irradiations carried out at the LCD laboratory.

Date	$H^*(10)$(μSv/h)	source	Activity (GBq)	Source-detector distance (m)
2015/02/06 12:10	2	Cs-137	0.336	4.008
2015/02/06 12:15	2	Cs-137	0.336	4.008
2015/02/06 12:20	2	Cs-137	0.336	4.008
2015/02/06 15:20	10	Cs-137	3.50	5.913
2015/02/06 15:25	10	Cs-137	3.50	5.913
2015/02/06 15:55	50	Cs-137	3.50	2.674
2015/02/06 16:00	50	Cs-137	3.50	2.674
2015/02/06 16:15	200	Cs-137	34.51	4.140
2015/02/06 16:20	200	Cs-137	34.51	4.140
2015/02/06 16:55	2000	Cs-137	510.4	4.772
2015/02/06 :17:00	2000	Cs-137	510.4	4.772
2015/03/17 17:35	0.72	Am-241	7.0	4.000
2015/03/17 17:40	0.72	Am-241	7.0	4.000
2015/03/17 17:45	0.72	Am-241	7.0	4.000
2015/03/27 14:50	0.72	Am-241	7.0	4.000
2015/03/27 14:55	0.72	Am-241	7.0	4.000
2015/05/14 13:50	5.22	Co-60	0.407	6.5
2015/05/14 13:55	5.22	Co-60	0.407	6.5
2015/05/15 14:15	5.22	Co-60	0.407	6.5
2015/05/15 16:25	12.3	Co-60	0.407	4
2015/05/15 16:30	12.3	Co-60	0.407	4
2015/05/15 16:55	22.5	Co-60	0.407	3
2015/05/15 17:00	22.5	Co-60	0.407	3
2015/05/15 17:15	52.2	Co-60	0.407	2
2015/05/15 17:20	52.2	Co-60	0.407	2

2.4. Irradiations at UDO II

Background spectra were recorded in June 2014 at the Underground Laboratory for Dosimetry and Spectrometry (UDO II) of the Physikalisch-Technische Bundesanstalt (PTB) in order to determine the inherent background of the detector. This laboratory is an ideal place for ultra-low-background γ-ray spectrometry as it has background radiation levels lower than 2 nSv h^{-1}. A description of the underground laboratory can be found in Neumaier and Dombrowski (2014).

2.5. Methods to calculate H*(10)

In this section the codes and methods employed to calculate $H^*(10)$ rates used by the UPC and CIEMAT are described.

2.5.1. 'spc2dose' computer code

The *'spc2dose'* code is a set of Fortran programs that calculates the $H^*(10)$ rate from photon pulse-height spectra. Unfortunately, it is unable to manage all the different possible formats of the spectra files. Therefore, users frequently find themselves having to adapt an existing code in order to meet their requirements. The package provides a modular code that can be adapted, thus significantly reducing programming effort . Currently, the code can manage the file formats for the ISO N42.42 standard (https://www.nist.gov/programs-projects/ansiieee-n4242-standard), as well as for PHD defined by the CTBTO (Preparatory Commission for the Comprehensive Nuclear-Test-Ban Treaty Organization, 2004).

The user has different options in order to calculate $H^*(10)$ rate from a specific series of spectra. Currently, stripping and conversion coefficients methods described in Sections 2.5.3 and 2.5.4 are included in *'spc2dose'*. The user can choose different options for computing the $H^*(10)$ rate in the input file. The code then generates an output file which provides the measurement time and the calculated $H^*(10)$ rate. Furthermore, for the stripping method, the calculated stripped spectra are also saved. For each acquired spectrum, a file containing the contribution to $H^*(10)$ rates for each energy bin is also stored for further studies. The different programs included in the *'spc2dose'* package have been written in Fortran 95 and are both free and open-source and can currently be obtained from the main author of this publication.

2.5.2. 'DET-H10R' computer code

The 'DET-H10R' is a code written in free Pascal for the calculation of ambient dose equivalent rates from measured photon pulse-height spectra. The code incorporates the ML-EM algorithm, described in Section 2.5.5, and the stripping method (Camp and Vargas, 2014) to obtain the incident photon fluence spectra by deconvoluting the measured pulse-height spectra using the response matrix of the detector. The ambient dose equivalent rates are then calculated using both the fluence spectra and the live acquisition time of the spectrometer. The calculated spectra of the incident photon fluence rate, air kerma rate and $H^*(10)$ rate can be saved to text files.

The file formats for the measured pulse height spectra provided by the spectrometric detectors can either be ISO N42.42 or binary CNF from CANBERRA. Furthermore, a code-specific text format is also defined for measured pulse-height spectra with formats that are not supported by the code.

A convolution algorithm has also been included to take into account the energy resolution of the detector during the application of the ML-EM method. The MC response matrix can be convolved with a spreading operator. This operator was constructed from the detector FWHM function using the Box-Müller algorithm (Box and Müller, 1958) and is normalized so that the counting statistics in the response matrix are not altered. The detector energy resolution can thus be incorporated into the response matrix in order to obtain more realistic incident fluence spectra.

A graphic user interface, including user help, facilitates the selection of the detector response matrix, the measured pulse-height spectra, the deconvolution method and the relevant calculation parameters, as well as the correct interpretation of the obtained results. The interface uses graphic tools to analyze both the measured pulse-height spectra and the calculated $H^*(10)$ rate spectra, thus facilitating the verification of the correct energy calibration of spectrometers and the identification of possible energy shifts due to spectrometer thermal instability.

2.5.3. Stripping method

The description presented in this section is an upgrade of the paper by Camp et. al 2014. The stripping method is based on calculating the incident fluence rate from the measured pulse-height spectrum from which the $H^*(10)$ rate can be obtained. Basically, the stripping method consists of subtracting all partial absorptions produced in the detector from the experimental spectrum in order to have only full absorptions. Once the spectrum has been stripped, the full-energy peak efficiency for each bin is used to estimate both the external ambient fluence rate and the absorbed dose rate. Thus, this method only requires knowledge of detector geometry and materials which have a direct influence on partial absorptions, while external parameters become unnecessary.

In order to apply the stripping method, the detector response should be isotropic since the incident angular fluence rate is not known. Isotropy of the detector has been previously evaluated by irradiations at different angles. Fig. 2 shows the angular relative response for the SpectroTRACER at different energies. The detector shows an almost isotropic response from 90° to ~ −30° (330°), while after this breakpoint efficiency drops to nearly zero at −90° (270°). The reason for this is the absorption produced by the electronics of the detector, located at the bottom half of the cylindrical housing, as can be seen in Fig. 1. The energies used for the study correspond to ^{241}Am, ^{137}Cs and ^{60}Co sources. The detector shows a different response for angles between the top face and the lateral face, i.e., 90° and 0° respectively. The difference is less than 10% for ^{137}Cs and ^{60}Co and is approximately 25% for ^{241}Am. This difference could be explained for the ^{241}Am source by the difference in the projected surface from the top and lateral face, which is about 20% for a cylindrical detector with the same length and diameter. In the case of higher energies, i.e, for ^{137}Cs and ^{60}Co, the probability of interaction per unit length becomes lower than for ^{241}Am photons and, therefore, the potential distance travelled by the gamma particle within the detector has to be taken into account. In the case of a cylindrical geometry this distance could be rather short for some of the incident photons and, therefore, probability of interaction would be low. This effect compensates the larger lateral projected surface and explains the smaller differences for ^{137}Cs and ^{60}Co sources.

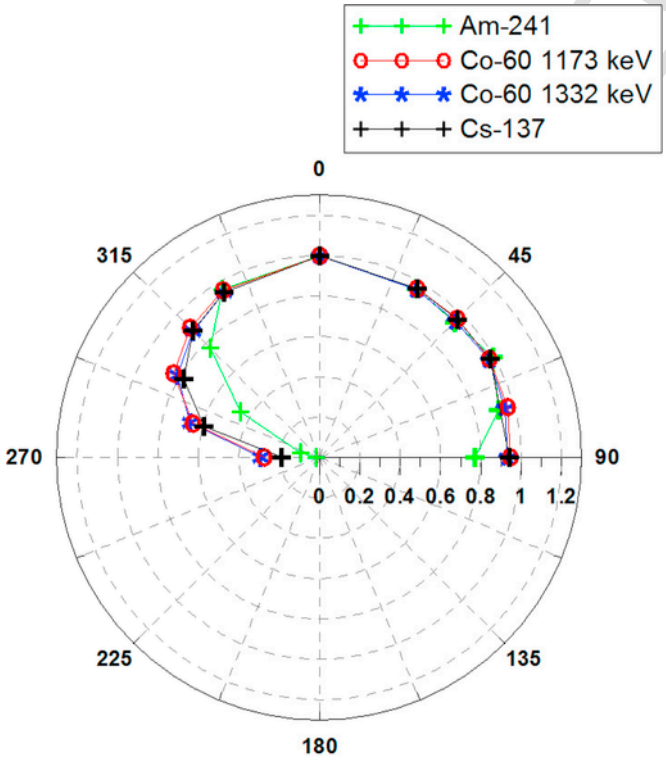

Fig. 2. Angular response of the SpectroTRACER using ^{137}Cs, ^{241}Am and ^{60}Co sources at LCD.

The following steps show the method used to calculate the partial absorptions produced in the detector for different energy fluences.

1. Simulations of monoenergetic parallel beams are performed in steps of 10 keV over an energy range from 0 to 3000 keV, i.e. 300 simulations, with an energy bin width of 0.5 keV.
2. The energy bins of the simulated spectra (0.5 keV) are grouped in 10 keV bins.
3. The detected counts in a bin i produced by a monoenergetic beam of energy j, $n_{j,i}$, are divided by the detected counts in the full-energy (FE) peak j as follows:

$$s_{j,1} = \frac{n_{j,1}}{n_{j,j}}, \quad s_{j,2} = \frac{n_{j,2}}{n_{j,j}}, \quad \dots s_{j,i} = \frac{n_{j,i}}{n_{j,j}} \dots, \quad s_{j,j-1} = \frac{n_{j,j-1}}{n_{j,j}}, \quad s_{j,j}$$

In order to find the stripped counts, firstly the net spectrum is calculated by subtracting the background spectrum measured at UDO II from the measured spectrum. The procedure to obtain the stripping spectrum and to estimate both the fluence rate and the $H^*(10)$ rate is described below:

1. The energy bins of the net spectrum are grouped in 10 keV energy bins, so that net spectrum and simulated spectra have the same bin width.
2. The stripped counts are iteratively calculated starting from the highest energy bin by using Eq. (2) (Miller, 1984).

$$N'_i = N_i - \sum_{j=i+1}^{n} N'_j \cdot s_{j,i}, \tag{2}$$

where N'_i are the counts in energy bin i due to full-energy absorptions, N_i are the counts detected in this energy bin i in the net spectrum and N'_j are the counts left after the last stripping cycle in the energy bins with higher energy than bin i (j values range from $i+1$ to n, where n is the energy bin with the highest energy gamma line).

1. The incident fluence rate, ϕ_i, in h^{-1} cm^{-2}, for each energy bin i is calculated from the counts in the stripped spectrum using the fol-

lowing equation:

$$\phi_i = \frac{N'_i}{\varepsilon_i \cdot t}, \tag{3}$$

where t is the spectrum measuring time in hours and ε_i is the FE peak efficiency per incident fluence rate in cm^2 for energy bin, i, which is calculated using Eq. (4):

$$\varepsilon_i = p_i \quad \Delta E_i S, \tag{4}$$

where p_i is the detection probability per incident gamma photon in bin i and unit energy in eV^{-1}, obtained from MC simulations, ΔE_i is the bin width in eV, and S is the surface area of the incident fluence rate in the Monte Carlo simulation, in cm^2.

2. Finally the $H^*(10)$ rate ($\mu Sv\,h^{-1}$) is calculated from the incident fluence rate using Eq. (5).

$$\dot{H}^*(10) = 1.602\ 10^{-10} \sum_{i=1}^{n} F_i\ \phi_i\ E_i\ \mu_i^{\text{air}} \tag{5}$$

where F_i is the conversion coefficient from air-kerma into ambient dose equivalent for energy bin, i, (ISO 4037-3, 1999), E_i is the energy of the particular energy bin (eV) and air μ_i^{air} is the mass energy transfer coefficient for air ($cm^2\ g^{-1}$) obtained from the NIST Standard Reference Database (Hubbell and Seltzer, 2004).

2.5.4. Conversion coefficients method

A description of this method can be found elsewhere, such as in Dombrowski (2014). The spectrum is divided into several energy regions and its corresponding conversion coefficient is applied to convert the count rate detected in the energy region to $H^*(10)$ rate. The total $H^*(10)$ rate results from the sum of m partial energy region contributions according to the following equation:

$$\dot{H}^*(10) = \sum_{i=1}^{m} w_i\ n_i\ E_i, \tag{6}$$

where w_i is the conversion coefficient for energy region i ($nSv\,h^{-1}/s^{-1}$ keV) , n_i is the count rate in s^{-1} in the region i for the measured spectrum and E_i *is* the mean energy of the energy region i in keV.

The conversion coefficients (w_i) are determined by MC simulations using PENELOPE/penEasy. The count rate in each energy region was calculated by simulating parallel beams normally incident to the central axis of the detector with energy corresponding to the midway energy of the specific energy region. The *H*(10)* rate for each energy fluence rate was obtained by using the values of the mass energy transfer coefficient in air (Hubbell and Seltzer, 2004) together with values of the conversion coefficient from the air kerma to the ambient dose equivalent from ISO 4037-3 (1999). For the energy bin with the lowest energy, the first coefficient is obtained by using the following equation:

$$w_1 = \frac{\dot{H}^*(10)_1}{E_1 \quad n_{11}}, \tag{7}$$

where n_{11} is the count rate in energy region 1, when the detector is exposed to a $H^*(10)_1$ rate produced by an incident fluence rate with an energy value that is midway in the first energy region. The generalized Eq. (8) is used for the next conversion coefficients:

$$w_i = \frac{\dot{H}^*(10)_i - \sum_{j=1}^{i-1} n_{ij} E_j w_j}{n_{ii} E_i}, \tag{8}$$

where n_{ij} is the count rate in region j, when the detector is exposed to a $H^*(10)_i$ rate produced by an incident fluence rate corresponding to the i-th energy region. Chosen energy regions used to carry out the Monte Carlo simulation and the corresponding calculated conversion coefficients are shown in Table 2.

2.5.5. ML-EM method

A Maximum Likelihood Estimation using the Expectation Maximization (ML-EM) algorithm is implemented in the 'DET-H10R' code to calculate incident photon spectra from the measured pulse height spectra.

The observed pulse height spectrum, $\vec{O}$, can be represented as:

$$\vec{O} = \hat{R} \bullet \vec{\Phi} \text{with} \left\{ \left(r_{i,j} \right) \in \quad \mathbb{R}^{n \text{x} m} \right\}, \tag{9}$$

where $\vec{\Phi}$ is the incident photon fluence spectrum and $\hat{R}$ is the detector response operator, for fluence spectra of dimension "m" and measured pulse-height spectra of dimension "n". Each element $r_{i,j}$ of the response operator represents the number of counts expected in channel i of the measured pulse-height spectrum per unit fluence of photons with energy in bin j.

The unknown fluence spectrum $\vec{\Phi}$ in Eq. (9) generates, and is to be calculated from, the measured pulse height spectrum $\vec{O}$ by using a known detector response operator, $\hat{R}$.

For each incident fluence spectrum, $\vec{\Phi}$, the measured spectrum, $\vec{O}$, has a probability or likelihood:

$$\mathrm{L}\left(\vec{O}\right) = \mathrm{p}\left(\vec{O}\vec{\Phi}\right) \tag{10}$$

The statistical approach described in Shepp and Vardi (1982) and Meng and Ramsden (2000) employing an Expectation Maximization algorithm has been used to find the solution of the Eq. (9), i.e. the fluence spectrum which gives the maximum probability value in Eq. (10).

From the response operator $\hat{R}$ the total efficiency operator $\hat{R}_{\mathrm{T}}$ is constructed, where $r_{\mathrm{T}\ i=j}$ are the elements of a diagonal matrix, representing the total number of photons detected per unit photon fluence in energy bin j, i.e. the total number of counts expected in the mea-

Table 2
Conversion coefficients calculated for the SpectroTRACER monitor using the PENELOPE/penEasy MC code.

photon energy (keV)	conversion coefficient ($nSv\,h^{-1}/s^{-1}$ keV)
40	7.84E-03
60	2.21E-03
80	1.69E-03
100	1.62E-03
130	1.49E-03
180	1.64E-03
250	1.89E-03
400	2.71E-03
630	3.76E-03
870	4.03E-03
1150	3.93E-03
1500	3.85E-03
2000	3.68E-03
2500	3.31E-03
2900	2.99E-03

sured spectrum per unit photon fluence in energy bin j ($r_{T\,i,j} = 0$ for $i \ddagger j$).

The vector of incident and detected photons $\overrightarrow{O}$ can thus be expressed as a function of the fluence vector $\vec{\Phi}$ using the total efficiency operator, $\hat{R}_T$, according to the following equation:

$$\overrightarrow{O} = \hat{R}_T \bullet \vec{\Phi} with \left\{ \left(r_{Ti,j} \right) \in \quad \mathbb{R}^{mxm} \right\} \tag{11}$$

From Eqs. (9) and (11), the following relationship can be deduced:

$$\vec{O} = \hat{R} \bullet \quad \hat{R}_T^{-1} \bullet \quad \overrightarrow{O} \tag{12}$$

That is:

$$\begin{aligned} \vec{O} = \hat{C} \quad \bullet \quad \overrightarrow{O} \Big\{ \hat{C} \\ = \hat{R} \bullet \quad \hat{R}_T^{-1} \Big\} with \left\{ \left(c_{i,j} \right) \right. \\ \in \quad \left. \mathbb{R}^{nxm} \right\}, \end{aligned} \tag{13}$$

where $\hat{C}$ is the conditional probability operator, and $c_{i,j}$ is the conditional probability that a detected photon, incident with energy j, is measured in channel i.

According to (11), for a given operator, $\hat{R}_T$, the solution of Eq. (9) that maximizes the likelihood function indicated in (10) provides the maximization of the likelihood:

$$\acute{\mathrm{L}} \left(\vec{O} \right) = \mathrm{p} \left(\vec{O} \overrightarrow{O} \right) \tag{14}$$

The Expectation Maximization (EM) algorithm is used to find the vector $\overrightarrow{O}$, for which the probability of having measured the spectrum $\vec{O}$ reaches the maximum value. Starting with an initial estimate, $\acute{O}_j^{r=0} \geq 0 \{ j = 1, \ldots, m \quad (n \quad \geq m) \}$, for which $\sum_{j=1}^{m} O_j'^{r=0} = \sum_{i=1}^{n} O_i$ the following EM iterative procedure is applied:

$$O_j'^{r} = O_j'^{r-1} \cdot \sum_{i=1}^{n} \frac{O_i \cdot c_{i,j}}{\sum_{s=1}^{m} O'^{r-1}_{s} \cdot c_{i,s}} \quad \{ j = 1, \ldots, m \} \tag{15}$$

The measured spectrum $\vec{O}$ could be taken as an initial estimate of $\overrightarrow{O}$ when $n = m$.

At each step the likelihood, p, increases, i.e., $\mathrm{p} \left(\vec{O} \overrightarrow{O}^{r} \right) \geq \mathrm{p} \left(\vec{O} \overrightarrow{O}^{r-1} \right) \{ r \geq 1 \}$. The incident photon fluence spectrum is calculated using the equation:

$$\vec{\Phi}^{r} = \hat{R}_T^{-1} \bullet \overrightarrow{O}^{r} \tag{16}$$

The ambient dose equivalent spectrum is calculated at each step r from $\vec{\Phi}^{r}$ using the values of the mass energy transfer coefficient in air from Hubbell and Seltzer (2004) together with the values of the conversion coefficient for air kerma to the ambient dose equivalent from ISO 4037–3 (1999).

The iterative process stops when

$$\Delta \quad = \quad \frac{H^*(10)^r - H^*(10)^{r-1}}{H^*(10)^{r-1}} \leq \delta, \tag{17}$$

where δ is the accepted relative deviation or the "Iteration resolution", defined by the user.

The incident fluence rate, the air kerma rate and the ambient dose equivalent rate are then calculated by using the total time taken to obtain the results.

The ML-EM does not require square matrices i. e. the number of energy values for $H^*(10)$ calculations could be a different value to the number of channels in the measured spectrum. The solution is always positive i.e. the components of the calculated incident spectrum are either zero or positive and the algorithm has very quick convergence, i.e. fractions of a second for δ values of the order of 10^{-5} on a standard CPU.

3. Results

3.1. Inherent background and LCD background

The inherent background of a $LaBr_3$ detector is mainly due to the ^{138}La and ^{227}Ac impurities in the crystal. A detailed description to evaluate this contamination can be found in Camp et al. (2016). Table 3 shows the calculated $H^*(10)$ rate for the different methods using a series of spectra acquired at UDO II. The uncertainty was calculated using the standard deviation of the measured spectra and are presented for a 95% confidence interval.

In the case of the LCD, there were other contributions to the background, apart from the inherent background, such as terrestrial and cosmic components, radon progeny concentrations in air and the contribution from artificial sources in the laboratory. The terrestrial component does not change significantly. The contribution of the cosmic component for such a detector is less than $10\,nSv\,h^{-1}$ according to experimental measurements carried out in lakes (internal discussion at MetroERM meetings) and, consequently, variations of the cosmic component do not significantly affect the measured $LaBr_3$ spectra at the LCD. As regards radon progeny, calculated conversion coefficients per unit air concentration in $nSv\,h^{-1}$ per $kBq\,m^{-3}$ were 0.607 and 2.063 for ^{214}Pb and ^{214}Bi in a $20\,m^3$ radon chamber (Kessler et al., 2017). In addition, calculations of conversion coefficients per unit deposited activity on the walls in $nSv\,h^{-1}$ per $kBq\,m^{-2}$ were 0.542 and 1.784 for ^{214}Pb and ^{214}Bi, respectively. Therefore, in order to have a conservative uncertainty value of the $LaBr_3$ $H^*(10)$ rate background at the LCD, a constant value of $2\,nSv\,h^{-1}$ was assumed with a 95% confidence interval. Table 4 shows the calculated $H^*(10)$ rates for the different methods using a series of spectra acquired at LCD.

Table 3
Inherent background measured at UDO II and background measured at the LCD facility. Statistical uncertainty is expressed with 95% confidence intervals.

Method	$H^*(10)$ / $nSv\,h^{-1}$	
	Inherent background	**LCD background**
STRIPPING	112.1 ± 0.6	159 ± 2
CONVERSION	88.0 ± 0.5	145 ± 2
ML-EM	86.8 ± 0.7	147 ± 2
Software MANUFACTURER	97.15 ± 0.08	159 ± 2

Table 4
Comparison of methods to calculate $H^*(10)$ rates for ^{137}Cs, ^{60}Co and ^{241}Am irradiations at the LCD facility. Uncertainty is expressed as the expanded uncertainty with a 95% confidence interval.

Radionuclide	Method $H^*(10)$ / μSv h^{-1}			
$H^*(10)$(reference) / μSv h^{-1}	Stripping	Conversion	ML-EM	Software Manufacturer
Cs-137				
2.00 ± 0.12	2.15 ± 0.05	2.021 ± 0.008	2.018 ± 0.018	2.161 ± 0.008
10.0 ± 0.6	10.6 ± 0.3	10.1 ± 0.2	10.2 ± 0.4	10.72 ± 0.10
50 ± 3	52.9 ± 1.2	50.7 ± 0.3	51.1 ± 1.1	53.4 ± 0.9
200 ± 12	224 ± 6	214 ± 2	213 ± 5	222 ± 6
2000 ± 118	2358 ± 13	2276 ± 10	2140 ± 9	2132 ± 8
Co-60				
5.2 ± 0.5	5.09 ± 0.02	5.19 ± 0.02	4.99 ± 0.05	5.517 ± 0.016
12.3 ± 1.2	13.7 ± 0.5	14.0 ± 0.4	13.41 ± 0.09	14.63 ± 0.15
22.5 ± 2.2	24.8 ± 0.7	25.7 ± 0.6	24.38 ± 0.01	26.43 ± 0.08
52 ± 5	58.2 ± 1.8	55.1 ± 0.3	57.0 ± 0.9	61.8 ± 1.2
Am-241				
0.72 ± 0.06	0.683 ± 0.002	0.662 ± 0.002	0.688 ± 0.004	1.114 ± 0.002

3.2. Irradiations at the LCD facility

A comparison of the results obtained by applying the different methods to calculate $H^*(10)$ rates for ^{137}Cs, ^{60}Co and ^{241}Am irradiations is shown in Table 4. The $H^*(10)$ rates represent the average values of the different $H^*(10)$ rates calculated from the spectra listed in Table 1. The uncertainties of the calculated values include the statistical uncertainty and the LCD background. The uncertainty of the reference values provided by the calibration laboratory includes the following components: uncertainty of the reference air kerma rate, uncertainty of the air kerma to ambient dose equivalent conversion coefficients, uncertainty of the long term stability of the reference standards, uncertainty given by beam non-homogeneities and uncertainty in instrument positioning, amongst the most important components.

Table 4 shows good agreement among the different methods used to calculate $H^*(10)$ rates compared to the reference values provided by the laboratory. Only at the highest $H^*(10)$ rate of 2 mSv h^{-1} do all the methods overestimate $H^*(10)$ rates and this is probably because of the higher contribution of the pile-up gammas and the measurement dead-time, which are not properly corrected by the spectrometer software.

Another issue that should be pointed out is that the method used by the manufacturer gives slightly higher $H^*(10)$ rates, except for ^{241}Am photons, for which the overestimation is significant.

3.3. ESMERALDA station

Fig. 3 shows the calculated $H^*(10)$ rates using stripping, conversion coefficients and ML-EM methods together with the calculated $H^*(10)$ rate values provided by the instrument using the manufacturer's algorithm and the Reuter-Stokes ionization chamber (RSS) at the ESMERALDA station (Sáez Vergara, 2016). In order to compare the $H^*(10)$ rates calculated using the different methods and the RSS chamber, a constant value of 45 nSv h^{-1} was subtracted from the RSS measured values. This constant value corresponds approximately to the contribution of cosmic radiation to the RSS. It should be also pointed out that this RSS unit is not temperature compensated. Therefore, it is not possible to carry out a precise comparison analysis with the RSS, but including this ionization chamber in the study is useful in order to have a rough comparison of "classical" dose meters and spectrometric detectors.

Fig. 3 shows that the general pattern of the different methods for $H^*(10)$ rate calculations are similar. The dispersion of the calculated

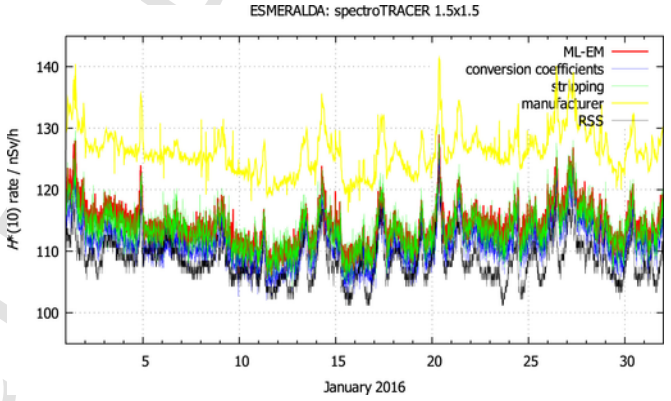

Fig. 3. $H^*(10)$ rates calculated with ML-EM , conversion coefficients, stripping and values downloaded from the monitor together with the data from the RS monitor during January 2016.

$H^*(10)$ rates is similar for ML-EM and conversion coefficients methods, while it is slightly higher for the stripping method. In contrast, the data provided by the manufacturer's algorithm has very low dispersion due to some kind of smoothing algorithm applied internally. The bias that can be seen in the figure will be commented on below.

The energy calibration curve of each spectrum provided by the manufacturer, included in the ISO N42.N42 files, is a second-order polynomial. As shown in Fig. 4, the coefficients provided by the manufacturer change suddenly for some periods and lead to steps in the calculation of $H^*(10)$ rates. Therefore, the coefficients of the second-order polynomial were re-calculated for ML-EM, conversion coefficients and stripping methods in order to obtain correct values of the $H^*(10)$ rate. This fact explains the $H^*(10)$ rate bias of the manufacturer's algorithm compared with the studied methods in the present work.

The 1465 keV peak produced by the inherent ^{138}La contamination was used for recalculating the coefficients of the energy calibration curve. For the calculations performed with the 'DET-H10R' code the peak produced by the inherent ^{138}La contamination was checked by visual inspection and was fitted to 1465 keV just when significant changes are observed in the energy calibration curve provided by the manufacturer. In case of the 'spc2dose' code, each spectrum was automatically corrected by fitting the ^{138}La contamination peak to a Gaussian curve. The channel corresponding to the centroid of the Gaussian distribution was then set to 1465 keV.

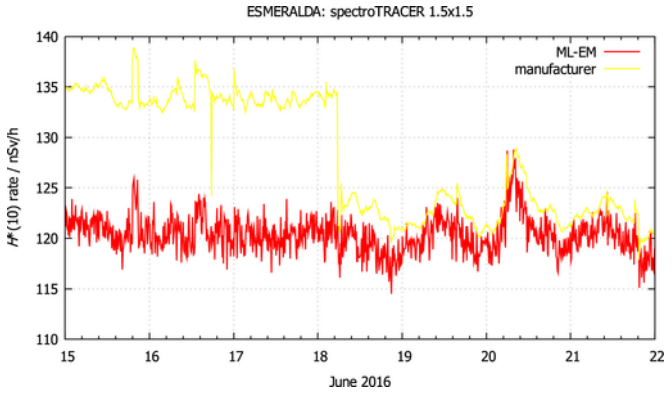

Fig. 4. $H^*(10)$ rates calculated with the ML-EM, conversion coefficients, stripping methods and values downloaded from the monitor together with the data obtained by the RS monitor during March 2016. The sharp variation in the $H^*(10)$ rates data downloaded from the monitor is a consequence of an incorrect energy calibration curve.

The effect of the small errors in the coefficients of the second-order polynomial equation provided by the manufacturer is clearly seen during hot summer periods. Fig. 5 shows $H^*(10)$ rates calculated with the ML-EM method with visual energy curve correction (red line), the conversion coefficients with corrected energy curve for each spectrum (blue line) and the same conversion coefficients method with uncorrected energy calibration curve (black line). In this figure it is clear that using the energy curve coefficients provided by the manufacturer (black line) produces a bias in the $H^*(10)$ rate calculations. Comparing the ML-EM method with visual correction and the conversion coefficients method using energy correction for each spectrum, a slightly different daily pattern is shown. This is explained by unobserved visually small shifts in the energy channels produced by temperature variations, which were corrected for each spectrum during the calculations carried out with the code 'spc2dose'. As can be seen in Fig. 5, when the calibration curve is corrected for each spectrum, the calculated $H^*(10)$ rates follow the radon progeny concentrations (orange line) more accurately.

The fluctuation in the $H^*(10)$ rate is mainly due to radon progeny concentration variations in the air and due to deposited radon progeny during rainy period. Fig. 6 shows both effects i.e., the radon air concentrations (days 1,2,3,5 and 6) and the increase in $H^*(10)$ rate due to rainy periods (day 7) for one week in February. Furthermore, during day 4 the effect of temperature on the RSS chamber is seen as it is not temperature compensated.

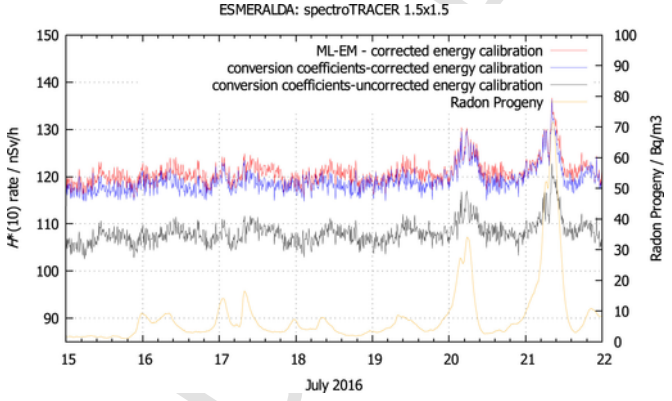

Fig. 5. $H^*(10)$ rates calculated with the ML-EM method with corrected energy calibration (red line), the conversion coefficients method with corrected energy calibration (blue line) and with the conversion coefficients method using the uncorrected energy calibration equation (black line) for one week in July 2016. Radon progeny pattern is also shown (orange line). (For interpretation of the references to color in this figure legend, the reader is referred to the web version of this article.)

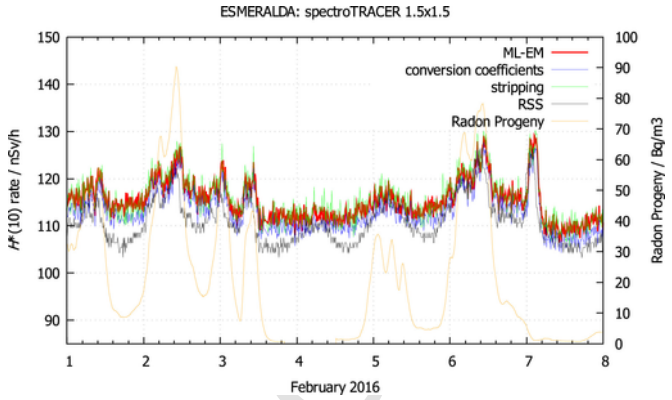

Fig. 6. $H^*(10)$ rates calculated with ML-EM, stripping and conversion coefficients methods, including the RSS measurements, for one week in February 2016. The increase of $H^*(10)$ due to air radon progeny concentration (days 1, 2, 3, 5 and 6) and due to a rainy period (day 7) is shown.

The figures in this section show a bias among the different methods. The bias between the ML-EM, conversion coefficients and stripping methods are quite small and are included in the uncertainties. As mentioned above, the bias of the $H^*(10)$ rate values using the manufacturer's algorithm is explained due to an error in the calculations of the energy curve coefficients. The bias of the RSS chamber can be explained due to the assumption of a constant value of $45\,\mathrm{nSv\,h^{-1}}$ and because the RSS has not been corrected for temperature.

4. Conclusions

The stripping, conversion coefficients, and ML-EM methods for calculating $H^*(10)$ from spectra acquired from the $LaBr_3(Ce)(1.5'' \times 1.5'')$ SpectroTRACER detector have been compared. Furthermore, the $H^*(10)$ rates with the manufacturer's algorithm have also been included in the comparison analysis. The comparison has been carried out at a secondary standard facility, which provided reference values of $H^*(10)$ rates for different energies and dose rates, and also at the ESMERALDA reference station, where there is a RSS chamber together with a radon progeny concentration device.

There is a good agreement between the different $H^*(10)$ rate calculation methods using the spectra measured at the LCD. The spectrometric detector works properly up to approximately $2\,\mathrm{mSv\,h^{-1}}$. For higher $H^*(10)$ rate values the detector does not provide correct spectra, nor do the calculation methods produce the expected results.

From the comparison analysis at the ESMERALDA station it can be concluded that all the methods give the same results and probably the best ones are the conversion coefficients and the ML-EM methods using re-calculated coefficients of the second-order polynomial energy calibration equation of each spectrum, due to a lower dispersion compared with the stripping method. On the other hand, the ML-EM and stripping methods also provide the fluence rate spectra, which are useful for radionuclide identification. It is therefore advisable for the manufacturers of spectrometric detectors to improve the calibration corrections required to compensate energy shifts due to gain changes associated with temperature variations. The bias between different methods is small except for the $H^*(10)$ rate values calculated by the manufacturer's algorithm, mainly because of insufficient energy-calibration stabilization.

The methods to calculate $H^*(10)$ rate from the spectrometric detector were compared with a RSS chamber installed at the ESMERALDA station. As indicated in Section 3.3, a constant value of $45\,\mathrm{nSv\,h^{-1}}$ was subtracted from the RSS. The RSS pressurized ion chamber is one of the most sensitive detectors for environmental radiation monitoring. However, due to its high price it is not normally installed at surveil-

lance stations. Less sensitive detectors are widely used, instead. From the study at ESMERALDA it can be concluded that the analysed methods to calculate $H^*(10)$ rates from the measured pulse-height spectra provide quite similar results to those obtained with the reference RSS ionization chamber, to within the associated measurement uncertainties. In addition, the spectrometric detectors can also facilitate radionuclide identification.

It is advisable to develop a plan to install spectrometric detectors at early warning stations in order to complement existing "classical" dosemeters.

reference

.

Acknowledgments

This work has been funded by EMRP within the JRP-contract number Env57 (MetroERM) project. The EMRP is jointly funded by EMRP participating countries within EURAMET and the European Union.

The authors would like to thank EURADOS (www.eurados.org), particularly Working Group 3, for their support in this research. Furthermore, we would like to thank María Roig and María Amor Duch at the UPC for carrying out the measurements at the LCD and José Carlos Sáez Vergara, Nuria Navarro Ortega, Gonzalo Benito Díaz and José Luis Márquez from CIEMAT for installing and operating the spectrometric detector at the ESMERALDA station and for providing both measurement data and relevant information from the station.

References

Box, G.E., Müller, M.E., 1958. A note on the generation of random normal deviates. Ann. Math. Stat. 29.

Camp, A., Vargas, A., 2014. Ambient dose estimation H*(10) from $LaBr_3$(Ce) spectra. Radiat. Prot. Dosim. 160 (4), 264–268.

Camp, A., Vargas, A., Fernández-Varea, J.M., 2016. Determination of LaBr3(Ce) internal background using HPGe detector and Monte carlo simulations. Appl. Radiat. Isot. 109, 512–517.

Dombrowski, H., 2014. Area dose rate values derived from NaI or $LaBr_3$ spectra. Rad. Port. Dosim. 160 (4), 269–276.

Hendricks, J.S.. et al. 2008. MCNPX 2.6.0 Extensions. LA-UR-08-2216 ⟨https://laws.lanl.gov/vhosts/mcnp.lanl.gov/pdf_files/la-ur-08-2216.pdf⟩.

Hubbell and Seltzer, 2004. Tables of X-Ray Mass Attenuation Coefficients and Mass Energy-Absorption Coefficients (version 1.4). [Online]Available: ⟨http://physics.nist.gov/xaamdi⟩. National Institute of Standards and Technology, Gaithersburg, MD.

International organization for standardization, 1999. X and gamma reference radiation for calibrating dosemeters and dose rate meters and for determining their response as function of photon energy. Part 3: Calibration of area and personal dosemeters and the measurement of their response as a function of energy and angle of incidence. ISO 4037-3.

Kessler, P., Camp, A., Dombrowski, H., Neumaier, S., Röttger, A., Vargas, A., 2017. Influence of radon progeny on dose rate measurements studied at PTB's radon reference chamber. Radiat. Prot. Dosim. https://doi.org/10.1093/rpd/ncx059.

Meng, L.J., Ramsden, D., 2000. An inter-comparison of three spectral-deconvolution algorithms for gamma-ray spectroscopy. IEEE Trans. Nucl. Sci. 47 (4).

Miller, K.M., 1984. A Spectral Stripping Method for a Ge Spectrometer Used for Indoor Gamma Exposure Rate Measurements. (USDOE publication, EML-419) Environmental Measurement Laboratory, New York.

Neumaier, S., Dombrowski, H., 2014. Eurados intercomparisons and the harmonisation of environmental radiation monitoring. Radiat. Prot. Dosim. 160, 297–305. https://doi.org/10.1093/rpd/ncu002.

Preparatory Commission for the Comprehensive Nuclear-Test-Ban Treaty Organization, 2004. IDC Documentation: Formats and Protocols for Messages. IDC-3.4.1Rev6, Vienna.

Sáez Vergara J.C., Romero A.M., Correa E., 1996. Establecimiento en el CIEMAT de una estación de referencia secundaria para la medida de dosis ambientales externas. In: Proceedings VI Congreso de la Sociedad Española de Protección Radiológica, Radioprotección (special issue), 153-154.

Sáez Vergara J.C., Vila Pena M., Sancho Llerandi C., 2004. CIEMAT/CSN Co-operation on the quality assurance of the Spanish automatic early-warning network 'REA'. 11th International Congress of the International Radiation Protection Association. Available at: ⟨irpa11.irpa.net/pdfs/6c33.pdf⟩.

Sáez Vergara J.C., 2016. Ambient dose equivalent rates measured with the ion – chamber Reuter Stokes RS112 at ESMERALDA Station. Personal communication in the framework of the EURAMET MetroERM project collaboration, Madrid.

Salvat, F., 2015. PENELOPE-2014. A code system for Monte Carlo simulation of electron and photon transport. OECD Nuclear Energy Agency. Data Bank NEA/NSC7DOSC3.

Sempau, J., Badal, A., Brualla, L., 2011. A PENELOPE-based system for the automated Monte Carlo simulation of clinacs and voxelized geometries—application to far-from-axis fields. Med. Phys. 38 (11).

Shepp, L.A., Vardi, Y., 1982. Maximum likelihood reconstruction for emission tomography. IEEE Trans. Med. Imaging MI-1 (2), .